Numerical Modeling of Wind Distribution Around a Tall Building in a 3D Urban Environment

M. Ahmadi, S.A.A. Mirjalily[*] and S.A.A. Oloomi

Department of mechanical engineering, Yazd Branch, Islamic Azad University, Yazd, Iran.

Abstract

This work applies an appropriate turbulence model in order to simulate the wind distribution in a 3D urban area around a tall building as a bluff body, which is one of the most important research topics due to the increasing concerns about the human health risks due to air pollution in the recent decades. The hybrid RANS-LES approach is used to reduce the computation time, while maintaining the computational accuracy. On the other hand, since no homogeneous direction exists in the flow in the hybrid (RANS-LES) approach, the LES and Smagorinsky Sub Grid-Scale (SGS) approaches are implemented with the standard k-ε turbulence model as RANS. In order to obtain more accurate results, the second-order Van Leer Method (VLM) is employed in advection terms. The sensitivity study of the input parameters shows that the intensity of the input turbulence has a significant effect on the surface pressure fluctuations. The results of velocity and pressure distribution show a very close agreement to the wind tunnel experimental data. Finally, the effects of the inflow characteristics on the peak pressure on the lateral sides are also studied. As a results, the fluctuation pressure distribution is strongly dependent on the turbulence of the flow.

Keywords: *Hybrid RANS-LES approach, Wind Distribution, Tall Building, Bluff Body, Pressure Distribution.*

1. Introduction

The study of wind distribution around buildings has become one of the most important research topics due to the increasing concerns about the human health risks and air pollution in the recent decades [1, 2]. The geometry of a building inevitably affects the climatic conditions of the environment inside and around it [3]. Especially in tall buildings, high winds around the building can be unpleasant and even dangerous for the people outside the building. Therefore, in designing the building, we should pay attention to the comfort conditions of the people inside the building and its impact on the outside environment [4]. In the flow modeling applications on the buildings, more attention is paid to the comfort of people inside the building, and attention to the effect of the wind outside the building is very little [5]. Also the outside conditions are considered in order to determine the boundary conditions of the wind on the building, and less attention is paid to the effect of wind on the climate around the building. The climate outside the building is affected by the wind speed, wind direction, rain, air pollution, radiation, and light [6-8]. These factors will change with the presence of the building and their change to the dimensions, shape, and direction of buildings as well as the impact of buildings on each other. These changes can be desirable or undesirable.

Wind interactions is one of the special environmental aspects that in the design of structures is considered. Davenport [9] has classified the aerodynamic of wind forces acting on a typical structure into three categories. The first is the load from the external sources such as hitting from natural wind or wakes of upstream obstacles. Secondly, the forces that act from the unstable flow phenomena such as separation [10], vortex collapse, and reattachments [11, 12]. Finally, the body motion that is induced, and is only suitable for the highly flexible structures.

Currently, the main goal of the engineers is to design and build the towers that reach new heights, while minimizing the construction costs [13]. These tall buildings have often narrow shapes, low natural vibration frequencies, and inherently structural damping value to increase

their sensitivity to wind agitations. These tall buildings often use narrow shapes, which have low natural vibration frequencies and inherently structural damping value, thus increasing their sensitivity to wind agitations. The effects of wind loading on tall buildings due to their wind-sensitive structures may lead to severe fatigue concerns [14] or affect the occupant comfort. In fact, they must be able to withstand natural wind so they combine two important characteristics [15]:

1. Flexibility: Reducing the density of the structure, while maintaining large dimension materials.

2. Bluff body aerodynamics: Make the designs more streamlined.

These two factors are the bases of aero elasticity and bluff body aerodynamics.

The idea of bluff body flow deduces from the kind of flow around the structure and its wake. An important character of the bluff body flows is separation of flow on its body surface [16, 17]. Wake dimensions are the same order of magnitude of the body. The drag force on the body is affected by the pressure distribution on the surface, while the viscous effects (skin friction) are not significant. The geometry of the bluff body is opposite to the streamlined body. The governing equations of these fluid flows are inherently unsteady, and a simple solution to these is usually not common. An important aspect to consider when analyzing the effects of wind on such structures is the turbulent regime of the wind. The atmospheric boundary layer that almost all structures are located is naturally turbulent. Significant amounts of literature have been devoted to describing this chaotic content. It is important to note that various turbulent characteristics of the oncoming flow have a significant effect on the flow around a bluff body and, in the case of a dynamic structure, the resulting structural response. The structures such as tall buildings are located on the ground, and therefore, situated within the boundary layer of the atmosphere. This area is almost always turbulent. Turbulence is, therefore, an inevitable factor in the design of the structures. Wind tunnel information is generally used to study the flow around a building but the CFD tools have also received a great deal of attention today with the proliferation of computers. The main advantage of the numerical methods is the reduction of wind tunnel costs but instead, they have the big disadvantage that they still require the wind tunnel results in order to validate the results, in addition to the 3D analysis of the turbulence regime around

several buildings. The limitations of computer processing are still very serious in more precise methods. There are generally three categories of methods for simulating a turbulent flow, which are:

-RANS

-LES

–Hybrid RANS-LES

Nowadays, the air pollution issue has turned into one of the biggest problems, especially in big cities, which has certain drawbacks on the human health, environment, and economy [18-20]. The turbulent wind flow around the buildings in urban areas is one of the best cases to evaluate the accuracy and efficiency of these turbulence models (RANS and LES) due to the physical complexities such as sharp corners, ground effect, various vortices formations, and other factors [21, 22]. In order to achieve accurate and reliable CFD results, validation for the study is mandatory, and the results obtained must satisfy specific criteria [23]. There are many CFD approaches in the simulation of flow around buildings. A review of the literature shows that the Large Eddy Simulation (LES) and the Reynolds-Averaged Navier-Stokes simulations (RANS) are the two most popular methods in this field [24-26]. Most such studies have used the RANS models to simulate pollutant distribution [27-31]; in contrast, the LES models are more suitable for estimating the wind flow in the atmospheric boundary layer and the dispersion of pollutants in the domain. The time-dependent nature of the results in the LES model reflects the fact that these models perform better than the RANS models in the steady wind flows around the buildings. For many decades, the Large Eddy Simulation (LES), which particularly could improve the flow prediction and offer more stable solutions, has been the only alternative to RANS [32-34].

In order to avoid the limitations of RANS and to take advantage of the benefits of LES, an important strategy in turbulent flow simulations is the hybrid RANS-LES approach, which has become increasingly popular in the past few years [35-38]. The basic idea of this approach is to increase the result accuracy and reduce the computational costs. The main aim of hybrid LES-RANS simulations is to apply the RANS equations in the inner layer near walls in order to avoid the need for an excessively fine grid required by the LES, whereas the LES equations are solve in the outer layer of a boundary layer [39-41]. In the recent years, many types of research works have been carried out in order to study the dispersion of pollutants around the

buildings. Tominaga *et al*. [42] have compared different models of k–ε with the Smagorinsky model and the experimental results. They concluded that the k–ε model did not have a sufficient accuracy in estimating the pollutant concentration. Their findings stated that the accuracy of the Smagorinsky averaged results were better than the k–ε results. The spread of gaseous pollutants around a cube-shaped building has been studied by Gousseau *et al*. [43]. They used the Smagorinsky model for simulation, and compared their findings with the results obtained from the wind tunnel. They affirmed that the results of the wind tunnel and the Smagorinsky model were in an excellent agreement.

The present paper continues this investigation by evaluating the wind disribution around a tall building as a bluff body, which is one of the most important research topics due to the increasing concerns about the human health risks due to air pollution in the recent decades. As mentioned, the methods used so far to model wind flow on buildings are either inaccurate (most RANS models such as the k-ε) or have a high execution time (LES models). For this reason, in this work, the hybrid RANS-LES approach is used to reduce the computation time, while maintaining the computational accuracy. On the other hand, since no homogeneous direction exists in the flow in the hybrid (RANS-LES) approach, the LES and Smagorinsky Sub Grid-Scale (SGS) models are implemented with the standard k-ε turbulence model as RANS. In this work, the following topics have been considered: 1. Analysis of the pressure coefficient distribution behind tall building caused with wind load distribution; 2. Analysis of the effects of turbulence on vortex formation (and its maximum pressures) on tall building; 3. Comparison of the result with the wind tunnel and experimental data.

2. Mathematical model

In this work, a numerical simulation is performed for the flow around an isolated tall model building (simulating a rectangular bluff body) in natural wind. The direction of the wind is assumed to be normal, and the windward is defined as the building surface. The stagnation point as the Bernoulli's principle is placed on this face, and approximately can be found at two-thirds of the building height [44]. The numerical simulation was made by the hybrid RANS-LES turbulence model. A classical model, as shown in figure 1, is chosen for the simulation. The computational dimensions were assumed to be 20.0H × 4.0H × 8.0H, and the building dimentions were the

streamwise lenght (L = H/6), width (W = H/3), and height = H, where H is the height of the building, and is considered as the reference length scale. Moreover, the boundary conditions are set in table 1. A no-slip boundary condition was applied to all the walls. The velocity was modelled with a wind power law exponent of α = 0.12 and set as $U(y) = U_H(y/H)^α$ with a value at y = 4H as U_H = 11.65 m/s. The Reynolds number was defined with the reference length (H) and the reference velocity (U_H) as Re = UH/ν, where ν is the kinematic viscosity of air, and considered as ν = 18.61 * 10^{-6} (m²/s). In this work, the Reynolds number was considered constant around Re = 3 * 10^5.

Table 1. Boundary conditions for computational domain.

Inlet	Outlet
U = U(y)	$\frac{\partial U}{\partial n} = 0$
$\frac{\partial p}{\partial n} = 0$	p = p∞

The well-known Finite Volume Method (FVM) was used to discretize the basic equations [45-47], and an in-house FORTRAN code was developed for the numerical solution of the case study based on the SIMPLEC algorithm. The number of time iterations and the time step were considered as 50000 and Δt = 10^{-4} second, respectively. This time step was selected since the Courant number must be less than one (CFL = uΔt/Δx) for stability, where Δx is the smallest grid size in the solution domain. The grid sizes are shown in table 2.
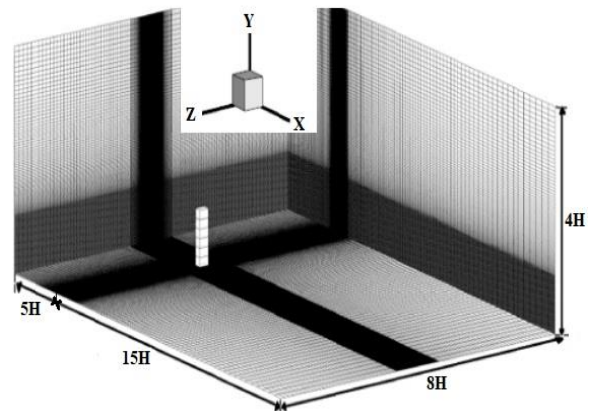

Figure 1. Geometry of problem.

2.1. Numerical method

The governing equations consist of a hybrid RANS-LES approach for the numerical solution of the fluid flow and the dispersion equations. The main equations were derived from the Navier-Stokes equations, which are the basic principles of

continuity and momentum conservations. All calculations were done at the constant temperature of 300 K. Also a 3D Cartesian coordinate system was applied in a steady, incompressible, and isothermal flow of a Newtonian fluid.

The governing equations for the standard k–ε turbulence model are expressed as follow:

Continuity equation [48-49]:

$$\frac{\partial \overline{U}_i}{\partial x_i} = 0 \tag{1}$$

Momentum equation [50-52]:

$$\overline{U}_j \frac{\partial \overline{U}_i}{\partial x_j} = -\frac{1}{\rho}\frac{\partial \overline{P}}{\partial x_i} + \frac{\partial}{\partial x_j}\left(v\frac{\partial \overline{U}_i}{\partial x_j} - \overline{u_i u_j}\right) \tag{2}$$

In equation (2), $\overline{U}_j$ and $\overline{u}_i$ are the mean and fluctuating components of the velocity, and U_i is the velocity in the x_i-direction. Also in the above equations, P is the mean pressure, ρ is the density, and v is the kinematic viscosity of the fluid.

The *K* and *ε* transport equations in the standard k–ε turbulence model follow as:

$$\frac{\partial K}{\partial t} + \overline{U}_j\frac{\partial K}{\partial x_j} = \frac{\partial}{\partial x_j}\left(\frac{v_t}{\sigma_k}\frac{\partial K}{\partial x_j}\right) + v_t\left(\frac{\partial \overline{U}_i}{\partial x_j}\right.$$
$$\left. + \frac{\partial \overline{U}_j}{\partial x_i}\right)\frac{\partial \overline{U}_i}{\partial x_j} - \varepsilon \tag{3}$$

$$\frac{\partial \varepsilon}{\partial t} + \overline{U}_j\frac{\partial \varepsilon}{\partial x_j} = \frac{\partial}{\partial x_j}\left(\frac{v_t}{\sigma_\varepsilon}\frac{\partial \varepsilon}{\partial x_j}\right) + \frac{\varepsilon}{k}\left(C_{\varepsilon 1}v_t\left(\frac{\partial \overline{U}_i}{\partial x_j}\right.\right.$$
$$\left.\left. + \frac{\partial \overline{U}_j}{\partial x_i}\right)\frac{\partial \overline{U}_i}{\partial x_j} - C_{\varepsilon 2}\varepsilon\right) \tag{4}$$

where:

$$\overline{u_i u_j} = \frac{2}{3}k\delta_{ij} - v_t\left(\frac{\partial \overline{U}_i}{\partial x_j} + \frac{\partial \overline{U}_j}{\partial x_i}\right) \tag{5}$$

$$v_t = C_\mu\left(\frac{k^2}{\varepsilon}\right) \tag{6}$$

K and ε are the turbulent kinetic energy and turbulent dissipation rate, respectively, v_t denotes the turbulent eddy viscosity, δ_{ij} is the Kronecker delta, and $C_\mu = 0.09$, $\sigma_k = 1.0$, $\sigma_\varepsilon = 1.314$, $C_{\varepsilon 1} = 1.44$, $C_{\varepsilon 2} = 1.92$ are the default constants for the standard k–ε turbulence model. The above constants were obtained from fine and exact data fittings over a wide range of common turbulent flows. The standard wall functions applies for the near-wall flow.

In the LES approach, using a spatial filtering operation, the large-scale and small-scale eddies of the flow will be separated so the large-scale eddies are solved directly, and the small-scale eddies are modeled and expressed as follow:

Continuity equation:

$$\frac{\partial \overline{U}_i}{\partial x_i} = 0 \tag{7}$$

Momentum equation [37-40]:

$$\frac{\partial \overline{U}_i}{\partial t} + \overline{U}_j\frac{\partial \overline{U}_i}{\partial x_j} = -\frac{1}{\rho}\frac{\partial \overline{P}}{\partial x_i} + \frac{\partial}{\partial x_j}\left(v\frac{\partial \overline{U}_i}{\partial x_j} - \tau_{ij}\right) \tag{8}$$

In equations 7 and 8, $\overline{U}_i$ is the filtered velocity, and $\overline{P}$ represents the pressure and not time-averaged values as in RANS equations. τ_{ij} is a tensor that represents due to the filtering operation, and it assumes that the small scales are more universal and isotropic than the large scales. τ_{ij} is called the Sub-Grid-Scale (SGS) stress, and is calculated from:

$$\tau_{ij} - \frac{1}{3}\tau_{kk}\delta_{ij} = -2\mu_t\overline{S}_{ij} \tag{9}$$

$$\overline{S}_{ij} = \frac{1}{2}\left(\frac{\partial \overline{U}_i}{\partial x_j} + \frac{\partial \overline{U}_j}{\partial x_i}\right) \tag{10}$$

$$\mu_t = \rho L_s^2|\overline{S}| \tag{11}$$

$$|\overline{S}| = \sqrt{2\overline{S}_{ij}\overline{S}_{ij}} \tag{12}$$

$$L_s = \min(kd, C_s V^{1/3}) \tag{13}$$

$\overline{S}_{ij}$ is the rate-of-strain tensor, μ_t the sub-grid-scale turbulent viscosity, L_s is the mixing length for the sub-grid scales, *k* is the Von Karman constant ($k = 0.4$), d is the closest wall distance, C_s is the Smagorinsky constant and set to 0.1, and V is the computational cell volume.

A linear interpolation based on the y^+ value is used for switching between RANS (k–ε) and the LES model, and it can be expressed as follows [53]:

$$v_t = \begin{cases} v_{t,LES} & \text{if} & y^+ > y_{up}^+ \\ (1-\beta)v_{t,K-\varepsilon} + \beta v_{t,LES} & \text{if} & y_{down}^+ < y^+ < y_{up}^+ \\ v_{t,K-\varepsilon} & \text{if} & y^+ < y_{down}^+ \end{cases} \tag{14}$$

$$\beta = \frac{y^+ - y_{down}^+}{y_{up}^+ - y_{down}^+} \tag{15}$$

β is the weight factor, and y_{down}^+ and y_{up}^+ are the lower and upper limits of the transition region, and selected as 60 and 300 [45].

2.2. Solution procedure

The hybrid RANS-LES model was employed in this work in order to simulate the turbulence effects. Discretization of the governing equations was carried out using the finite volume method [45-47] on a fully structured grid to conduct the numerical solution procedure. For the momentum equation discretization in LES, a second-order upwind-central numerical scheme was utilized for the space terms. For the standard k-ε model, the second-order central differencing scheme was used for the transport terms because it allows a clear separation between the convective and diffusive terms to discretize the momentum equation, turbulent kinetic energy (k), and turbulent dissipation rate (ε) equations. Furthermore, for the time marching, the implicit second-order method was applied. In order to achieve more accurate results, the second-order Van Leer approach was applied as a proper limiter in the advection simulation terms [54-55]. The SIMPLEC algorithm was selected to resolve the problem of velocity and pressure coupling. The number of outer correction was set 1, and 3 for pressure corrections. TDMA and the Strongly Implicit Procedure (SIP) algorithms were utilized for pressure correction, and the convergence criteria for all the flow parameters were set at 10^{-6}.

2.3 Grid study

During the simulation process, grid refinement is one of the most important issues to acquire accurate and reliable results, especially near the walls and fluid boundaries. As it was discussed earlier, a non-uniform and fully structured computational grid was selected. Equation (16) was used to create a compression near the walls.

$$y = H\frac{(2\alpha + \beta)\left(\frac{\beta + 1}{\beta - 1}\right)^{\frac{\gamma - \alpha}{1 - \alpha}} + 2\alpha - \beta}{(2\alpha + 1)(1 + \left[\left(\frac{\beta + 1}{\beta - 1}\right)^{\frac{\gamma - \alpha}{1 - \alpha}}\right])} \quad (16)$$

where α, β, and γ denote the location, parameter of compression, and nomber of divisions. A maximum stretching ratio of 1.05 was applied to reduce the grid density in the areas far away from the regions of interest. The Y^+ value near the walls was reduced to less than 5 by making the grid finer due to the presence of larger gradients in the solution variables. In order to ensure that the results were independent from the grid size,

two different mesh combinations were generated, and their details were tabulated in table 2.

Table 2. Mesh details; H is reference length.

Grid	Number of elements (x × y × z)		$\Delta x_{min}, \Delta y_{min}$	Δz_{min}
	Bottom up to top of building(H)	Free surface layer		
Coarse mesh	$140 \times 60 \times 80$	$140 \times 60 \times 70$	$4.19 \times 10^{-3}H$	$8.56 \times 10^{-3}H$
fine mesh	$180 \times 80 \times 120$	$180 \times 80 \times 90$	$1.83 \times 10^{-3}H$	$6.56 \times 10^{-3}H$

Both the experimental water channel and numerical results were selected for the grid study [56-57]. Figure 2 shows a comparison of the velocity distribution and velocity fluctuations at the centerline of a channel after a vertical bluff body. As it can be seen in this figure, the uniform fine grid certificats the results so the fine mesh is selected for the next calculations.
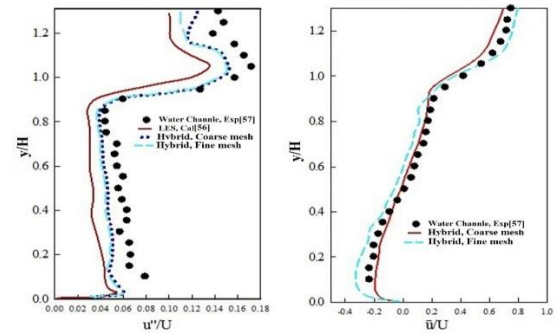

Figure 2. Comparison of velocity distribution and velocity fluctuations at the centerline of a channel after a vertical bluff body.

2.4 Validation

After selecting the appropriate grid, the numerical results obtained were compared against the experimental data from the open literature [59, 60]. The flow around a squard cylinder at four different Reynolds numbers was studied. The drag coefficient results from the hybrid model with the experimental data were examined. Figure 3 shows that the calculated results of the hybrid model are in good agreement with those obtained from the experiment but with a smaller magnitude.
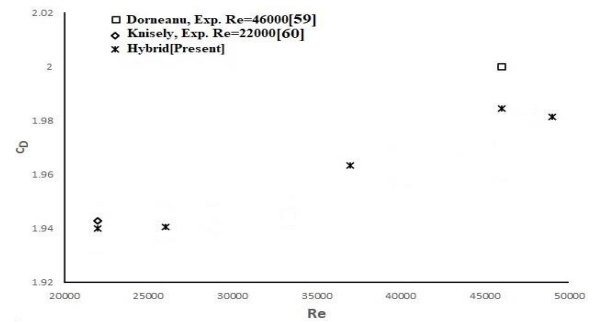

Figure 3. Comparsion of drag coefficient from current hybrid model with experimental data [59, 60].

The maximum diference was with 2.31% deviation. After this comparison, it could be concluded that the current turbulence model was capable of handling the flow and wind loading in an open environmental and around a bluff body (tall building). Furthermore, figure 2 can also be used as another validation for the results of this study against the results obtained by [56-57].

3. Results and Discussion

After selecting the appropriate grid and also ensuring the validity of the computer code, different runs were conducted with different models. The Reynolds number (Re) was assumed to be constant at $Re = 3 * 10^5$, and the geometrical parameters were fixed for all cases. In the following sections, the comparisons of the results obtained by the hyrid RANS-LES turbulence model are presented. In order to increase the quality of the hybrid results, the inlet flow based on the turbulence intensity factor, 5% was the turbulence according to equations 16 and 17.

$$TI=I=\frac{u^{'}}{U} \tag{16}$$

$$u^{'} = \sqrt{\frac{1}{3}(u_x^{'2} + v_x^{'2} + w_x^{'2})} \tag{17}$$

In the above equations, U is the inlet mean velocity, and $u^{'}$ is the velocity fluctuations. Firstly, a general compersion of the computations in term of velocity at the centerline of computer domain at the vicinity upstream of the tall building was analyzed for the previously mentioned model. Based on the distribution of the velocity profile, it could be seen that the mean velocity had an excellent agreement with the wind tunnel data by Dagnew and Bitsuamlak [58] and wind power law, as it could be seen in figure 4. Also figure 5 shows a comparision of the turbulence intensity with the wind tunnel data at the vicinity of the tall building. As it could be seen in this figure, the hybrid results of turbulence intensity were in agreement with the wind tunnel target profile for y > 0.2123H, with some little difference closer to the ground.

Then the mean velocity and mean pressure coefficients were extracted on the windward, sidewall, and leeward faces for the isolated building at y = 4/5H of the building for various inflow boundary conditions. The streamlines and velocity contours are shown in figures 6 and 7; it was seen that there were different flow patterns in the street canyons.

The streamlines and velocity contours are shown in figures 6 and 7. As shown in these figures, the

use of SGS in simulation of laminar sub-layer in the hybrid approach cause a noticeable change in the streamline and secondary flows. After the tall building, the vortices grow in both lateral sides and longitudinal directions, and the two longitudinal vortices meet at the approximate point x/H = 2.45 behind the tall building. Using the SGS model causes the velocity fluctuations modeled by the viscosity of the sublayer. Thus the length of velocity fluctuation will be reduced, and the Reynolds stresses will be correctly predicted. Thus the length of the vortices and their sizes will be simulated correctly. Due to the small width of the tall building, a large number of eddies enter this area, and on the other hand, the velocity fluctuations are high in this area and based on the necessity of this model in simulating these fluctuations and dumping them; in the lateral sides, it increases the laminar sub-layer. This increase leads to an increase in the vortex size and low-pressure area in the lateral sides.
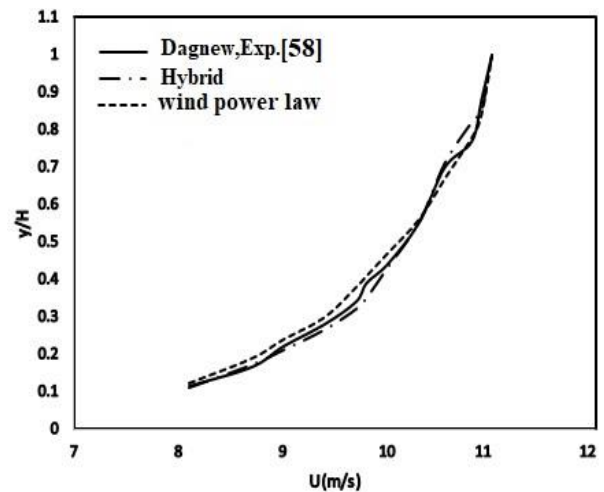

Figure 4. Comparision of velocity with wind power law and wind tunnel data at vicinity of the tall building.
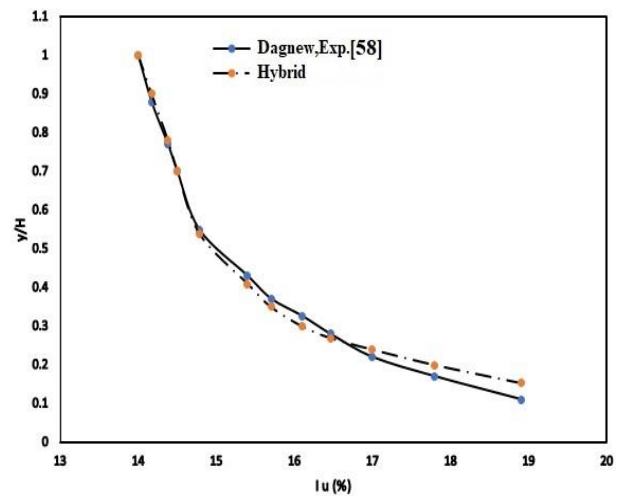

Figure 5. Comparision of turbulence intensity with wind tunnel data at vicinity of the tall building.
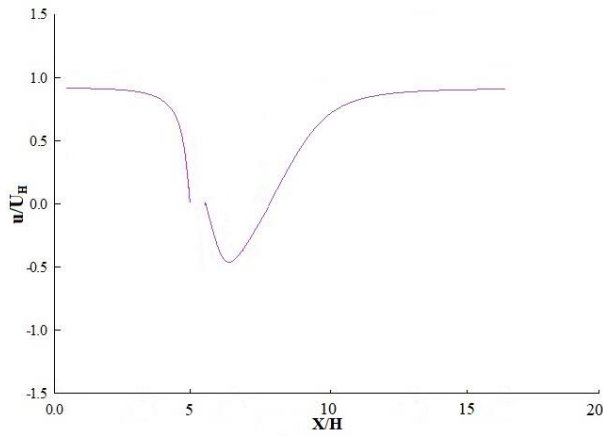
Figure 6. Mean velocity distribution over cross-section of tall building at the centerline and y = 4/5H.
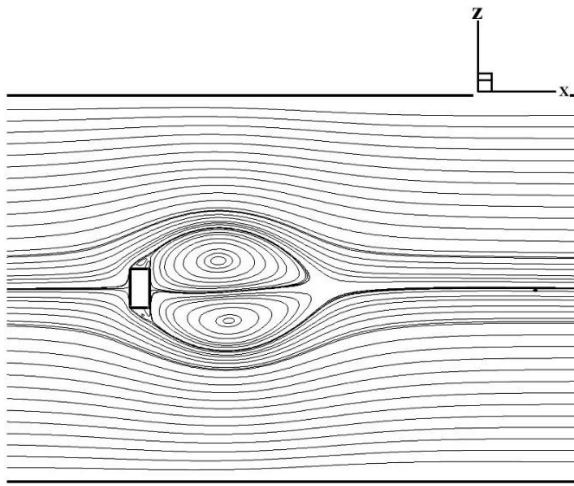
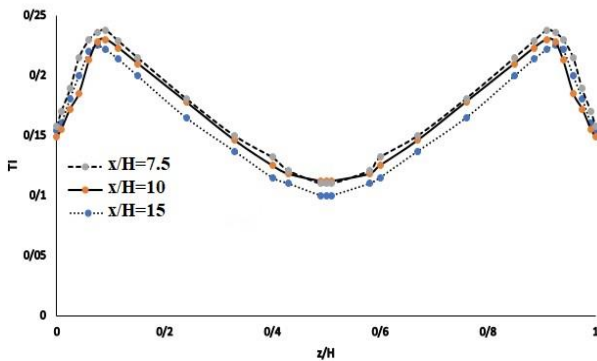**Figure 7. Mean velocity distribution over cross-section of tall building at the centerline and y = 4/5H.**

Figure 8. Axial turbulence intensity profiles predicted by hybrid model at the centerline and y = 4/5H at x /H = 7.5, 10 and 15.

As it could be seen in the figure 8, the axial turbulence intensities are highest near the walls and behind the tall building. By increasing the distance downstream, the tall building, and the proximity of the outlet, the turbulence intensity is more uniform, which is due to the damping effects of the wall. Comparing these profiles, it could be concluded that the hybrid approach predicts the Reynolds stresses with an acceptable percentage

of confidence. Due to the SGS combination, this model is able to more accurately predict and analyze the intensity of turbulence intensity near the walls as well as behind the tall building.
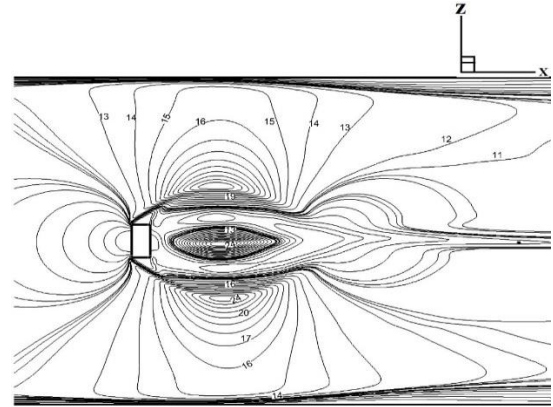
Figure 9. Pressure distribution over cross-section of tall building at the centerline and y = 4/5H.

Figure 9 showes the pressure distribution over the cross-section of the tall building at the centerline and y = 4/5H. This figure is in agreement with the velocity distribution in figures 6 and 7. As it could be seen in figure 9, the peak pressure towards the trailing edge could be attributed to the separated bubble in this region. At the corners with the peak pressure, another contradiction can be seen in the results, i.e. concerning whether the pressure fluctuations on the front face area at a maximum of minimum along the center. Goliger and Milford [61] offered that the broad range of turbulence intensities and experimental errors presented by many wind tunnel test may be the reason for the mutations in the pressure fluctuations on the front face of the tall building. For such geometries, as expected, due to the sharp edges, the flow separation points are known, and the Reynolds number has no significant effect on the average pressure coefficient distribution. In the geometry studied in this research work, the passing flow is separated from the upper and lower corners of the upstream face.
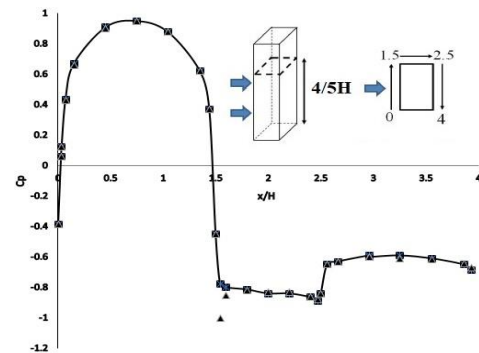
Figure 10. Pressure coefficient distribution over cross-section of tall building at the centerline and y = 4/5H. ∗ Dagnew, Exp.[58], ▲ Current hybrid method.

Due to the geometric symmetry of the tall building relative to the flow, the pressure distribution on the upper and lower surfaces is the same. As a result, the value of the mean pressure coefficient on these two surfaces is almost the same.
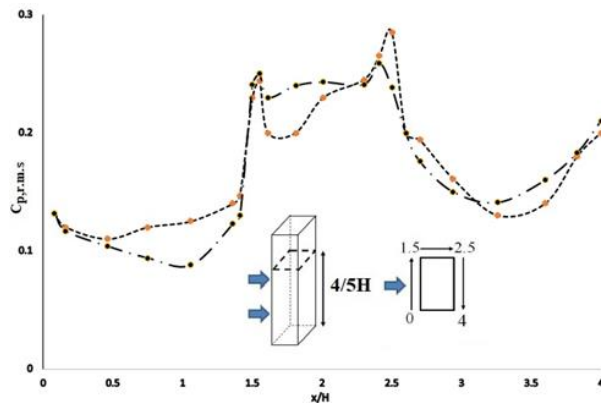

Figure 11. Root-mean-squard pressure fluctuation distribution over cross-section of tall building at the centerline and y = 4/5H. ● Dagnew, Exp. [58], -- Current hybrid method.

Figures 10 and 11 show a very close agreement with the experimental data [58] for all sides of tall building. By comparing the computed data with the experimental, it can be seen that the data is significantly scattered over the lateral sides. It may be due to the small variations in the inflow characteristics as the results (Figures 10 and 11) shown in the biggest discrepancy are in the calculation of the peak pressure at the leading and trailing edges often the former showing a larger discrepancy. The base settings for the mean velocity and turbulence intensity were derived from Dagnew [58] with the differences of the fluctuation pressures more are at the leading edges that could be adjectivized to the approximations for the turbulence length scales. These approximations were concluded for the pressure study.

4. Conclusions

In this work, we studied the wind disribution around a tall building as a bluff body; it is one of the most important research topics due to the increasing concerns about the human health risks due to air pollution in the recent decades. The hybrid RANS-LES approach was used in order to reduce the computation time, while maintaining the computational accuracy. The LES and Smagorinsky Sub-Grid-Scale (SGS) models were implemented with the standard k-ε turbulence model as RANS. Using the SGS model caused that the velocity fluctuations modeled by the viscosity of the sub-layer and thus the length of

velocity fluctuation was reduced, and the Reynolds stresses were correctly predicted. The artificial turbulent inlet condition was used in order to simulate the large vortices to predict the mean pressure and root-mean square (rms) pressure fluctuations on a tall building model. For a better modeling of the mean pressure, the new input conditions were proven. In the case of the rms. pressure, it can be cleared that the hybrid model simulated the free-stream wind loads and the corresponding suction pressures at the corners of the tall building. The sensitivity study of the input parameters shows that the intensity of the input turbulence has a significant effect on the surface pressure fluctuations. The results of the velocity and pressure distribution showed a very close agreement with the wind tunnel experimental data. Finally, the effects of the inflow characteristics on the peak pressure on the lateral sides were also studied. As a result, the fluctuation pressure distribution was strongly dependent on the turbulence of the flow.

References

[1] Davenport A.G. (1998). What makes a structure wind sensitive? In A.A. Balkema, The Jubileum Conference on Wind Effects on Buildings and Structures, Porto Alegre, Brazil, 1998.

[2] Zaniani J.R. et al. (2015). Examining the Possibility of using Solar Energy to Provide Warm Water using Retscreen4 Software (Case Study: Nasr Primary School of Pirbalut), Special Issue of Curr World Environ,10 (Special Issue May 2015).

[3] Mostafaeipour A. et al. (2019). Energy efficiency for cooling buildings in hot and dry regions using sol-air temperature and ground temperature effects, Journal of Engineering, Design and Technology, Vol. 17, No. 3, pp. 613-628.

[4] Almutairi K. et al. (2021). Frontiers in Energy Research, Techno-Economic Investigation of using Solar Energy for Heating Swimming Pools in Buildings and Producing Hydrogen: A Case Study, doi.org/10.3389/fenrg.2021.680103.

[5] Jahangiri M. et al. (2019). An optimization of energy cost of clean hybrid solar-wind power plants in Iran, International Journal of Green Energy, Vol. 16, No.15, pp. 1422-1435.

[6] Jahangiri M. et al. (2019). Techno-econo-environmental optimal operation of grid-wind-solar electricity generation with hydrogen storage system for domestic scale, case study in Chad, International Journal of Hydrogen Energy, Vol. 44, No. 54, pp. 28613-28628.

[7] Moradi cheghamahi J. et al. (2019). Numerical solution of the Pulsatile, non-Newtonian and turbulent blood flow in a patient specific elastic carotid artery,

International Journal of Mechanical Sciences, Vol. 150, pp. 393-403.

[8] Jahangiri M. et al. (2018). Comprehensive Evaluation of using Solar Water Heater on a Household Scale in Canada, Journal of Renewable Energy and Environment, Vol. 5, No. 1, pp. 35-42.

[9] Qiao Z.X. et al. (2021). Multi-frequency aerodynamic control of a yawed bluff body optimized with a genetic algorithm, Journal of Wind Engineering and Industrial Aerodynamics, 212104600.

[10] Minelli, G. et al. (2019). Active aerodynamic control of a separated flow using streamwise synthetic jets. Flow, Turbul. Combust, Vol. 103, No. 4, pp.1039–1055.

[11] Brunton S.L. et al. (2020). Machine learning for fluid mechanics, Annu. Rev. Fluid Mech, Vol. 52, pp. 477–508.

[12] Owan J. et al. (2013). Fifty years of wind engineering: prestige lectures from the sixth European and African conference of wind engineering, University of Birmingham.

[13] Tamura Y. (2009). Wind-induced damage to buildings and disaster risk reduction. In the seventh Asia-Pacific conference of wind engineering, Taipei, Taiwan.

[14] Andrianne T. (2012). Experimental and numerical investigation of the aeroelastic stability of bluff bodies. PhD thesis. Department of Aerospace and Mechanics. University of Liege.

[15] Minelli, G. et al. (2020). Upstream actuation for bluff-body wake control driven by a genetically inspired optimization, J. Fluid Mech, Vol. 893, pp. 1–28.

[16] Bonnavion, G. et al. (2019). Boat-tail effects on the global wake dynamics of a flat backed body with rectangular section, J. Fluid Struct, Vol. 89, pp. 61–71.

[17] Brook R.D. et al. (2004). Expert Panel on P, Prevention Science of the American Heart A. Air pollution and cardiovascular disease: a statement for healthcare professionals from the Expert Panel on Population and Prevention Science of the American Heart Association, Circulation, Vol. 109, pp. 2655–2671.

[18] Jahangiri M. et al. (2018). Electrification of a Tourist Village using Hybrid Renewable Energy Systems, Sarakhiyeh in Iran, Journal of solar energy research, Vol. 3, No. 3, pp. 201-211.

[19] Jahangiri M. et al. (2018). Analysis of Standalone PV-Based Hybrid Systems for Power Generation in Rural Area, ICEEC01_166.

[20] Pahlavan S. et al. (2019), Assessment of PV-based CHP System: The Effect of Heat Recovery Factor and Fuel Type, Journal of Energy Management and Technology (JEMT), Vol. 3, No. 1, pp. 40-47.

[21] Li Z. et al. (2021). Review on pollutant dispersion in urban areas-part B: Local mitigation strategies, optimization framework, and evaluation theory. Build Environ, Vol. 198, 107890.

[22] Gao NP. et al. (2009). The airborne transmission of infection between flats in high-rise residential buildings: particle simulation, Build Environ, Vol. 44, pp. 402–410.

[23] Allegrini J. et al. (2018). Simulations of local heat islands in Zurich with coupled CFD and building energy models, Urban Climate, Vol. 24, pp. 340–359.

[24] An K. et al. (2013). Sensitivity of inflow boundary conditions on downstream wind and turbulence profiles through building obstacles using a CFD approach. Journal of Wind Engineering and Industrial Aerodynamics, Vol. 115, pp 137–149.

[25] Antoniou N. et al. (2017). CFD and wind-tunnel analysis of outdoor ventilation in a real compact heterogeneous urban area: Evaluation using "air delay", Building and Environment, Vol. 126, pp. 355–372.

[26] Bazdidi-Tehrani F. et al. (2013). Grid resolution assessment in large eddy simulation of dispersion around an isolated cubic building, Journal of Wind Engineering and Industrial Aerodynamics, Vol. 121, pp. 1–15.

[27] Blocken B. et al. (2007a). CFD simulation of the atmospheric boundary layer: Wall function problems, Atmospheric Environment, Vol. 41, pp. 238–252.

[28] Tian ZF. et al. (2006). On the numerical study of contaminant particle concentration in indoor air flow, Building and Environment, Vol. 41, pp. 1504–1514.

[29] Ahmadi M. et al. (2019). RANS k-ω simulation of 2d turbulent natural convection in an enclosure with heating sources, IIUM Engineer Journal, Vol. 20, No. 1, pp. 229–244.

[30] He C. et al. (2017). A dynamic delayed detached-eddy simulation model for turbulent flows, Comput Fluids, Vol. 146, pp. 174-189.

[31] Wang M. et al. (2012). Advanced turbulence models for predicting particle transport in enclosed environments, Building and Environment, Vol. 47, pp. 40–49.

[32] Mirjalily SAA. (2021). Lambda shock behaviors of elliptic supersonic jets; a numerical analysis with modification of RANS turbulence model, Aerospace Science and Technology, Vol. 112, 106613.

[33] Baker CJ. (2007). Wind engineering-Past, present and future. Journal of Wind Engineering and Industrial Aerodynamics, Vol. 95, pp. 843-870.

[34] Meroney RN. (2016). Ten questions concerning hybrid computational/physical model simulation of wind flow in the built environment, Building and Environment, Vol. 96, pp. 12-21.

[35] Ahmadi M. (2017). Natural Convective Heat Transfer in a Porous Medium within a Two-Dimensional Enclosure, IIUM Engineering Journal, Vol. 18, No. 2, pp. 196–211.

[36] Tominaga Y. et al. (2016). Ten questions concerning modeling of near-field pollutant dispersion in the built environment, Building and Environment, Vol. 105, pp. 390-402.

[37] Meroney RN. et al. (2014). Virtual reality in wind engineering: the windy world within the computer, Journal of Wind Engineering and Industrial Aerodynamics, Vol. 11, pp. 11-26.

[38] Jinglei X. et al. (2017). A dynamic hybrid RANS/LES approach based on the local flow structure, Int J Heat Fluid Flow, Vol. 67, pp. 250-260.

[39] Shur ML. et al. (2015). An enhanced version of DES with rapid transition from RANS to LES in separated flows, Flow Turbul Combust, Vol. 95, No. 4, pp. 709-737.

[40] Mockett C. et al. (2017). Go4Hybrid: Grey Area Mitigation for Hybrid RANS-LES Methods: Results of the 7th Framework Research Project Go4Hybrid, Funded by the European Union, 2013-2015. Berlin, CT: Springer-Verlag.

[41] Allmaras SR. et al. (2012). Modifications and clarifications for the implementation of the Spalart-Allmaras turbulence model, Paper presented at: Proceedings of the 7th International Conference on Computational Fluid Dynamics, pp.1-11.

[42] Tominaga Y. et al. (2010). Numerical simulation of dispersion around an isolated cubic building: model evaluation of RANS and LES, Building and Environment, Vol. 45, pp. 2231-2239.

[43] Gousseau P. et al. (2011). CFD simulation of pollutant dispersion around isolated buildings: on the role of convective and turbulent mass fluxes in the prediction accuracy, Journal of Hazardous Materials, Vol. 192, pp. 422.

[44] Bi A. (2006). Probability assessment of wind loads on a full-scale low-rise building, PhD thesis, Texas Tech University, United States.

[45] Patankar SV. (1980). Numerical Heat Transfer and Flow, McGraw-Hill, New York.

[46] Ferziger JH. et al. (1996). Computational Methods for Fluid Dynamics. Springer; Verlag, Berlin.

[47] Launder BE. et al. (1972). Lectures in Mathematical Models of Turbulence. Academic Press, London, England.

[48] You D. et al. (2007). A Dynamic Global-Coefficient Sub Grid-Scale Eddy-Viscosity Model for Large-Eddy Simulation in Complex Geometries, Phys Fluids, Vol. 19, No. 6, 065110–18.

[49] Jahangiri M. et al. (2015). Effects of Non-Newtonian Behavior of Blood on Wall Shear Stress in an Elastic Vessel with Simple and Consecutive Stenosis, Biomedical and Pharmacology Journal, Vol. 8, No. 1, pp. 123-131.

[50] Moradi cheghamahi J. et al. (2019). Numerical solution of the Pulsatile, non-Newtonian and turbulent blood flow in a patient specific elastic carotid artery, International Journal of Mechanical Sciences, Vol. 150, pp. 393-403.

[51] Jahangiri M. et al. (2015). Numerical simulation of hemodynamic parameters of turbulent and pulsatile blood flow in flexible artery with single and double stenoses, Journal of Mechanical Science and Technology, Vol. 29, No. 8, pp. 3549-3560.

[52] Sharifzadeh B. et al. (2020). Computer modeling of pulsatile blood flow in elastic artery using a software program for application in biomedical engineering, Computer Methods and Programs in Biomedicine, Vol. 192, 105442.

[53] Sajjadi H. et al. (2017). Turbulent Indoor Airflow Simulation using Hybrid LES/RANS Model Utilizing Lattice Boltzmann Method, Comput Fluids, Vol. 150, pp.66–73.

[54] Ahmadi M. et al. (2020). Simulation of Pollutant Dispersion in Urban Street Canyons using Hybrid RANS-LES Method with Two-Phase Model, Computers and Fluids, Vol. 210, 104676.

[55] Ahmadi M. et al. (2020). CFD Simulation of Non-Newtonian Two-Phase Fluid Flow through a Channel with a Cavity, Thermal science, Vol. 24, No. 2B, pp.1045–54.

[56] Li XX. et al. (2008b). Physical modeling of flow field inside urban street canyons, J Appl Meteorol Climatol Vol. 47, No. 7, pp.2058–2067.

[57] Liu CH. et al. (2004). Large-eddy simulation of flow and pollutant transport in street canyons of different building-height-to-street-width ratios, J Appl Meteorol, Vol. 43, pp. 1410–1424.

[58] Dagnew AK. et al. (2010). LES evaluation of wind pressure on a standard tall building with a without a neighboring building, In the Fifth International Symposium on Computational Wind Engineering (CWE2010), Chapel Hill, North Carolina, USA, pp. 23-27.

[59] Dorneanu J. et al. (2016). Hirschberg, Tonal and silent wake modes of a square rod at incidence, ACTA Acustica United with Acustica, Vol. 102, No. 3, pp. 419-422.

[60] Knisely CW. (1990). Strouhal numbers of rectangular cylinders at incidence: a review and new data, Journal of Fluids and Structures, Vol. 4, No. 4, pp. 371-393.

[61] Goliger A.M. et al. (1988). Sensitivity of the caarc standard building model to geometric scale and turbulence, Journal of Wind Engineering and Industrial Aerodynamics, Vol. 31, No. 1, pp.105-123.